Collision energy dependence of the HD($\nu'=2$) product rotational distribution of the H+D$_2$ reaction in the range 1.30–1.89 eV

Florian Ausfelder, Andrew E. Pomerantz, and Richard N. Zare[a)]
Department of Chemistry, Stanford University, Stanford, California 94305-5080

Stuart C. Althorpe
Department of Chemistry, University of Exeter, Stocker Road, Exeter EX4 4QD, United Kingdom

F. J. Aoiz, Luis Bañares, and Jesus F. Castillo
Departmento de Química Física, Facultad de Química, Universidad Complutense, 28040 Madrid, Spain

(Received 29 September 2003; accepted 20 November 2003)

An experimental and theoretical investigation of the collision energy dependence of the HD($\nu'=2,j'$) rotational product state distribution for the H+D$_2$ reaction in the collision energy range of $E_{col}=1.30$–1.89 eV has been carried out. Theoretical results based on time-dependent and time-independent quantum mechanical methods agree nearly perfectly with each other, and the agreement with the experiment is good at low collision energies and very good at high collision energies. This behavior is in marked contrast to a previous report on the HD($\nu'=3,j'$) product state rotational distribution [Pomerantz *et al.*, J. Chem. Phys. **120**, 3244 (2004)] where a systematic difference between experiment and theory was observed, especially at the highest collision energies. The reason for this different behavior is not yet understood. In addition, this study employs Doppler-free spectroscopy to resolve an ambiguity in the $E,F-X$ resonantly enhanced multiphoton ionization transition originating from the HD($\nu'=2,j'=1$) state, which is found to be caused by an accidental blending with the transition coming from the HD($\nu'=1,j'=14$) state.
 [DOI: 10.1063/1.1641009]

I. INTRODUCTION

The hydrogen exchange reaction in its various isotopic combinations has proven to be one of the most extensively studied bimolecular reactions. Its simplicity makes it a benchmark system for theoretical studies. This reaction is a likely system for more subtle quantum effects like dynamical resonances[1] and geometric phase.[2] For a review of recent theoretical work on this reaction system, see Althorpe and Clary.[3]

While being "simple" to study from a theoretical view point, this reaction has proven to be much harder to work with from an experimentalist's perspective. Nevertheless, numerous studies on different observables have been performed. In general, experimentalists used coherent-anti-Stokes–Raman spectroscopy (CARS),[4–9] resonance enhanced multiphoton ionization coupled with time-of-flight mass spectrometric detection (REMPI-TOF MS)[10–20] or H/D-atom Rydberg tagging[21–26] to probe the products of the reaction.

Recently, we measured the energy dependence of the HD($\nu'=3,j'$) product rotational distribution in the range of $E_{coll}=1.49$–1.85 eV and compared the observations with the results from the most advanced time-dependent and time-independent quantum mechanical methods.[20] Interestingly enough, the experimental observations deviated significantly and in a systematic manner from the theoretical predictions at high collision energies. To investigate this phenomenon further, we decided to extend the study to the collision energy dependence of the HD($\nu'=2,j'$) product rotational distribution.

Several experimental studies have already been performed for this product, mostly at a collision energy of 1.3 eV owing to the convenient photolysis of HI at 266 nm.[5,13,24] Studies using REMPI detection also report a strangely increased relative population in the HD($\nu'=2,j'=1$) product state[12] for high collision energies. In addition, several theoretical studies at different levels of theory and using different potential energy surfaces (PES) have been performed.[22,26–33]

One of the aims of this study is to clarify the behavior of the HD($\nu'=2,j'$) product rotational distribution over the collision energy range of 1.30–1.89 eV and to identify the source of the odd behavior for the $E,F-X$ REMPI transition originating from the HD($\nu'=2,j'=1$) state.[12] The major emphasis is placed, however, on comparing the experimental results over the entire energy range investigated to the most advanced time-dependent and time-independent quantum mechanical calculations.[20]

II. EXPERIMENT

The experimental setup is essentially the same as the one we used in a recent study.[18] Therefore, a general overview will be given and the important aspects and differences to the previous work[19,20] will be highlighted.

[a)]Author to whom all correspondence should be addressed. Electronic mail: zare@stanford.edu

A. General setup

The setup is standard for photoinitiated reactions with subsequent REMPI detection of the products. Figure 1(a) shows a schematic representation of the experimental setup. The experiments were conducted in a stainless steel vacuum chamber and run at a frequency of 10 Hz. A 10% mixture of HBr in D_2 is expanded via a supersonic expansion into the ionization region of a Wiley–McLaren TOF-MS perpendicular to the TOF axis. The expanding molecular beam is then intercepted at right angles with respect to the TOF axis as well as the expansion direction of the molecular beam by the photolysis laser beam to produce H and Br atoms. The H atoms then react with the D_2 in the expansion to form HD products. After a time delay of 5–18 ns between the firing of the photolysis laser and the probe laser, the latter selectively ionizes specific rovibrational states of the HD product. The HD ions are then extracted, accelerated, and, after passing through a drift region, detected by means of striking two multichannel plates (MCPs). The resulting ion signal is recorded by a digital oscilloscope (Tektronix TDS 620) and transferred to a computer for data storage and analysis.

B. Photolysis step

The photolysis laser beam is produced by using the second harmonic of a Nd:YAG laser (Quanta-Ray Cobra) to pump a dye laser (Quanta-Ray PDL-2) in order to produce an output in the range of 606–690 nm, which is then tripled and results in about 2–3 mJ of tuneable UV light between 202 and 230 nm. This beam passes through a focusing lens on a translational stage which allows one to keep the position and the focal conditions roughly constant when changing the photolysis wavelength.

The photolysis beam produces Br in two different spin–orbit states. The branching ratio depends on the wavelength of the photolysis beam. Under the conditions present in the experiment the relative yields are 85% $^2Br_{3/2}$, the spin–orbit ground state (Br) and about 15% $^2Br_{1/2}$, the spin–orbit excited state (Br*).[34] Therefore, two different kinds of H atoms are produced and the resulting collision energies for the reaction with D_2 differ by 0.35 eV.

The contributions of these two channels are not separated, and the observed signal is the weighted sum. In general, the resulting signal will be heavily weighted toward the fast channel, because it is not only preferentially produced by the photolysis but it also tends to be more reactive. We estimate the collision energy resolution to be about 50 meV.

C. Detection of the HD product via [2+1] resonance enhanced multiphoton ionization

The reaction of H atoms with D_2 forms HD products in various rovibrational states. After a short time delay between 5 and 18 ns the probe laser beam enters the chamber in order to detect that the HD($\nu'=2,j'$) products are state-specifically detected via [2+1] REMPI. The first two photons resonantly excite the molecule in the $E,F\,^1\Sigma_g^+ - X\,^1\Sigma_g^+$ (0,2) band, after which the third photon ionizes the molecule that is then detected in the Wiley–McLaren TOF-MS.

The probe laser beam is tuned to a specific rovibronic transition in the wavelength range of 216.5–223 nm. This wavelength range is produced by pumping a dye laser (LPD 3000) with the second harmonic of a Nd:YAG laser (Quanta-Ray GCR-3) to produce a laser beam in the range of 555.7–601 nm. This beam is then sum frequency mixed with residual light from the third harmonic of the Nd:YAG in a β-barium tetraborate (BBO) crystal having a cut angle of 65° to produce the desired wavelength range. This process has proven to be very reliable. It produces up to 10 mJ of UV light.[19,20] In this study we use average output energy of about 2 mJ per pulse. Again, the laser beam has to be focused into the reaction region and a translational stage is used to adjust for the change of focal conditions as a function of the probe laser wavelength. The Nd:YAG laser was equipped with an injection seeder and could be run in narrow bandwidth (seeded) or in broad bandwidth mode (unseeded mode); the latter was used to extract the rotational distributions. The resulting mixed UV laser beam bandwidth was estimated by scanning over a [2+1] REMPI Ar transition at 216.9 nm via the first electronically excited state of Ar. Due to the high mass of the Ar atom, the line is not significantly Doppler broadened, thereby allowing the use of the measured width of this transition as an upper limit on the effective laser bandwidth. Because even the unseeded bandwidth of the laser is much smaller than the bandwidth of the Doppler broadened transitions, the laser must be scanned over the whole Doppler profile of any given transition for measuring HD product states.

The REMPI process is highly power dependent and a careful study of the signal as a function of probe laser power, which is constantly recorded, allows us to correct the observed signal for shot-to-shot variations.[19]

An additional problem is caused by HBr photolysis from the probe laser. In order to correct for this unwanted signal, the REMPI line is measured at a small time delay between photolysis and probe laser pulses of 5 ns and at a longer time delay of 18 ns. The difference between those two signals is a true representation of the HD produced in the time difference of 13 ns. This treatment requires the production of HD to be in a linear regime during this time interval.[20]

Some of the HD REMPI transitions accidentally overlap with resonant bromine atom transitions. The resulting high density of charged particles leads to strong deviations of the flight path of the ions and interferes directly with the mass resolution and separation by the TOF system. This interference proved prohibitively strong for the transition originating from the HD($\nu'=2,j'=8$) state under normal experimental conditions. Fortunately, slightly defocusing the probe beam allowed one to change experimental conditions in a way that the HD($\nu'=2,j'=8$) transition could still be detected without too much interference from the bromine resonance, albeit sacrificing most of the signal. Therefore, the HD($\nu'=2,j'=8$) transition was usually measured with a slightly different arrangement. By measuring the adjacent transitions in both experimental conditions scaled to the rest of the data set it was possible to obtain a better measure of this signal strength. This procedure increases random but not systematic errors.

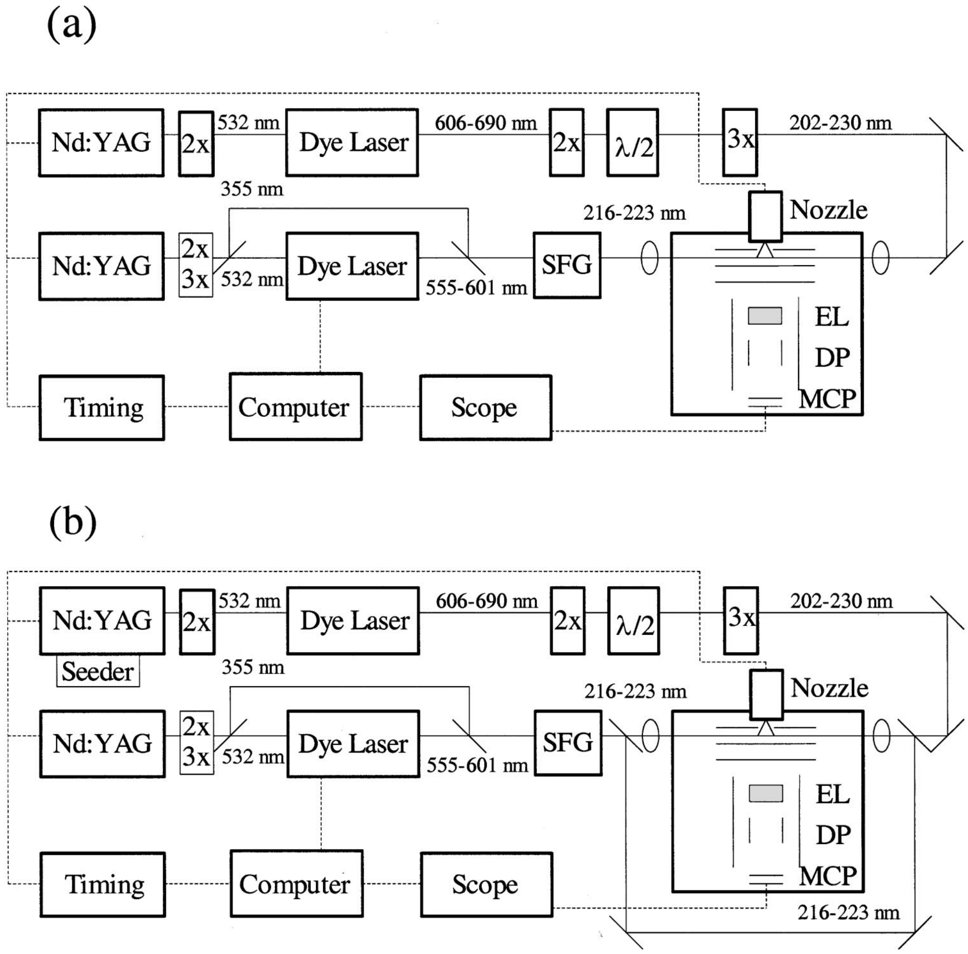

FIG. 1. Experimental setup as block diagram: (a) standard setup; and (b) setup used for Doppler-free scans. (SFG) Sum frequency generation, (EL) einzel lens, (DP) deflection plates, (MCP) multichannel plates.

D. Doppler-free REMPI detection of HD($\nu'=2,j'=1$)

In order to investigate the unusually high HD($\nu'=2,j'=1$) population reported in the literature[12] the experimental setup was changed slightly to allow for Doppler-free REMPI detection of the HD($\nu'=2,j'=1$) transition.[35] This setup is displayed in Fig. 1(b). The major changes to the setup were the use of the injection seeder on the probe laser side, which narrows the mixed UV laser bandwidth down to 0.3 cm^{-1} and the splitting of the probe beam into two approximately equal components by means of a 50% beamsplitter. The beams were counterpropagated and focused to one spot in the chamber after passing through optical delay lines to ensure spatial and temporal overlap in the detection region.

E. Estimating relative detection sensitivities

In order to convert measured ion signal intensities to state specific populations it is necessary to know the specific line strength of a given transition and the effect of various experimental parameters. The system can be calibrated on a known distribution and correction factors can be obtained for each rovibronic transition. One way of approaching the problem would be to measure HD($\nu'=2,j'$) produced by a thermal source[36] hot enough to produce all rovibrational states energetically allowed in the reaction. This was not suitable for this study because of the high temperatures required.

However, it is known from previous work[37] that HD expanded over a hot tungsten ion gauge filament dissociates and recombines to produce a wide variety of vibrational states. If the ambient pressure is chosen to be high enough for the average HD molecule to undergo enough collisions to relax rotationally, but not vibrationally, a thermalized rotational distribution in an excited vibrational level can be observed. Due to the large rotational constant of HD, this method only populates the HD($\nu'=2,j'=0-4$) states. The system can then be calibrated, at least of the low rotational levels on the observed thermal distribution. Figure 2 presents these results, which exhibit no significant deviation from a thermal distribution. These results are also in very good agreement with calculations of two-photon transition moments,[38] which were then taken as correction factors for the higher rotational levels.

F. Extracting rotational populations

A detailed discussion of this subject is found in an earlier publication[20] and only the actual analysis procedure will be given here. The recorded signals are corrected for baseline and probe laser power. Integration over the whole signal

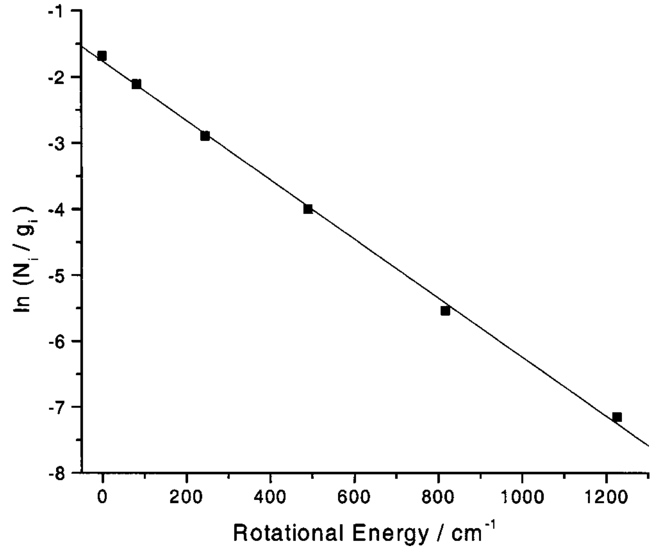

FIG. 2. Calibration of the REMPI lines: The points are the experimental data and the line is a linear fit to the Boltzmann plot which corresponds to a temperature of 321 ± 6 K.

leads to an area. The area of the signal recorded at 5 ns is then subtracted from the area of the signal recorded at 18 ns. This resulting area needs to be corrected for the detection sensitivity for the specific rovibrational level. This leads to a number that is proportional to the number of molecules produced in that delay time difference in the specific rovibrational state in the detection volume. This process is carried out for all rotational levels energetically accessible for a given collision energy. In order to adjust for long term drifts in the experimental setup, the rotational manifold was scanned in an upward direction, taking two scans over the Doppler profile for each transition for the short and long delay times, followed by the same procedure scanning the rotational manifold in a downward direction.

As discussed earlier, the conditions for measuring $j'=8$ were slightly different and the results were scaled with the help of the transitions of $j'=7$ and $j'=9$ transitions to yield the complete rotational distribution.

III. THEORETICAL METHODS

These experimental results are compared to time-dependent and time-independent calculations. All calculations used the Boothroyd–Keogh–Martin–Peterson surface II (BKMP2) potential energy surface (PES)[39] and were confined to the ground surface, neglecting all non-Born–Oppenheimer correction terms (such as the geometric phase effect).

A. Time-dependent quantum mechanical calculations

The time-dependent wave packet results were obtained using the method of Ref. 40, in which a quantum wave packet, containing a spread of energies, is propagated from the initial $A+BC$ ($H+D_2$) through to the final $AC+B$ (HD+D) arrangements of the reaction. Efficient basis sets are constructed from grids based on $A+BC$ Jacobi coordinates in the reagent approach region, and $AC+B$ coordinates in the transition-state and product exit regions. This method recently yielded the first rovibrationally resolved state-to-state cross sections to be calculated by time-dependent wave packet methods,[40] and has since been used to generate movies showing the scattering into space of the reaction products.[41–44]

The calculations used to generate the $00\rightarrow 2j'$ cross sections reported here used the same parameters as the calculations used to obtain the $00\rightarrow 3j'$ cross sections of reference 20. Wave packets were propagated for all values of the total angular momentum quantum number J between 0 and 30, using basis function grids that were sufficiently dense to converge individual fixed-J reaction probabilities to better than 2%. Results were obtained over a continuous range of collision energies from $E_{col}=0$ to 2.2 eV.

B. Time-independent quantum mechanical calculations

The time-independent quantum mechanical (QM) calculations were performed for the $H+D_2(\nu=0,j=0)$ reaction by means of a time-independent coupled-channel hyperspherical method[45] at the collision energies measured experimentally over the range 1.30–1.90 eV. The key parameters that define the coupled-channel basis set are E_{max}, j_{max}, and k_{max} (see Ref. 45). At the collision energies of the present work, well converged integral cross sections were obtained using the parameters $j_{max}=20$, $E_{max}=2.85$ eV, and $k_{max}=10$ and including all partial waves up to total angular momentum $J=36$. Using these parameters, the number of channels to be propagated ranges from 198 at $J=0$ up to 1532 at $J\geqslant 10$. A maximum value of the hyperradius $\rho_{max}=2.5a_0$ and a number of 250 sectors were selected to perform the calculations.

C. Quasiclassical trajectory calculations

In addition to the above-mentioned QM calculations, quasiclassical trajectory (QCT) calculations were performed for the $H+D_2(\nu=0,j=0,1,2)$ reactions on the same BKMP2 PES at 1.64 and 1.85 eV collision energies to check for the effect of the internal energy of the D_2 reagent on the product $HD(\nu'=2)$ rotational distributions. The QCT method employed in this work has been described elsewhere,[46] and only the details relevant to the present work will be given here. Batches of 10^6 trajectories were run at each collision energy and initial rotational quantum state of the D_2 reagent. Trajectories were started at a H–D_2 distance of 7 Å and a time step of 5×10^{-17} s was used, which guarantees conservation of the total energy to better than one part in 10^5 and conservation of total angular momentum to better than one part in 10^6. The maximum impact parameter employed was 1.35 Å in all cases. The rovibrational energies of the D_2 and HD molecules were calculated by semiclassical quantization of the classical action, using in each case the asymptotic diatomic potential of the PES.[46] The assignment of the final product quantum numbers was carried by equating the classical rotational angular momentum of the product molecule to $[j'(j'+1)]^{1/2}\hbar$. With the (real) j' value so obtained, the (real) vibrational quantum number ν' is found by equating the internal energy of the outgoing molecule to the

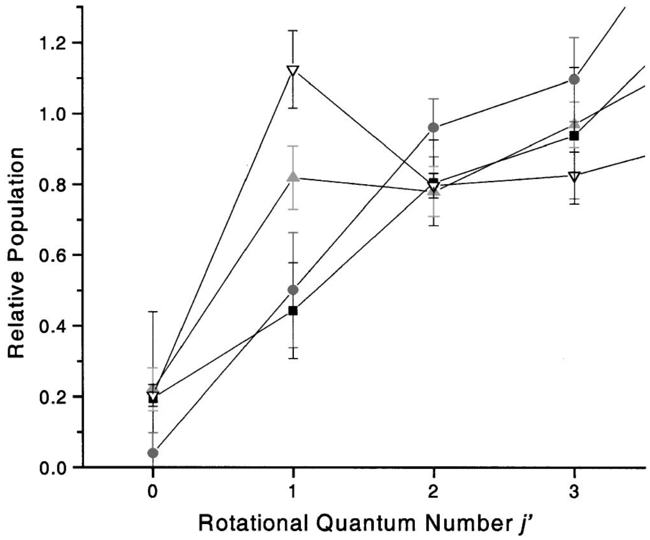

FIG. 3. Apparent growth of the relative population in the HD($\nu'=2,j'=1$) state as a function of collision energy: $E_{\mathrm{coll}}=1.54$ eV (black squares), 1.64 eV (gray circles), 1.80 eV (closed triangles) and 1.89 eV (open triangles). Populations are normalized to the sum of the HD($\nu'=2,j'=0$) and HD($\nu'=2,j'=2$) population.

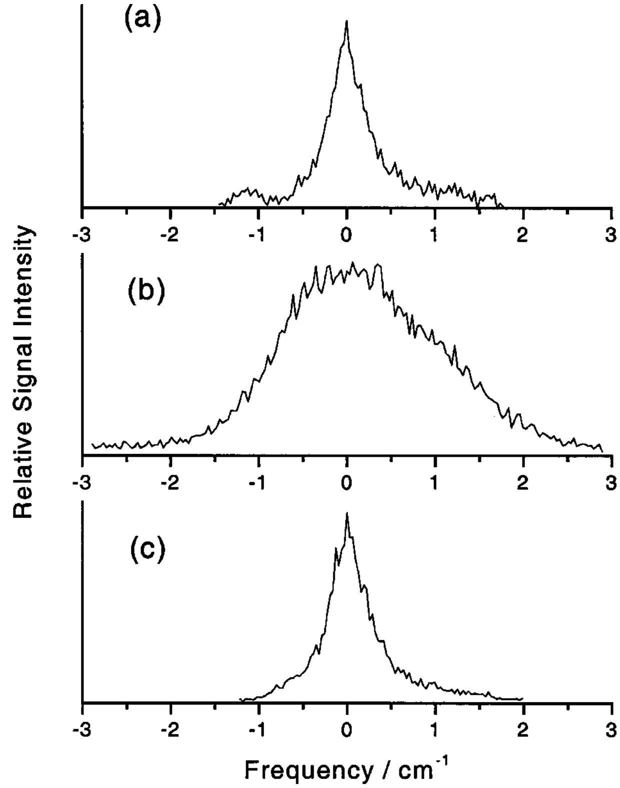

FIG. 4. Observed REMPI transitions originating from the (a) HD($\nu'=2,j'=0$), (b) HD($\nu'=2,j'=1$), and (c) HD($\nu'=2,j'=2$) states. The center of the transitions has been chosen to be the origin of the x axis.

corresponding Dunham expansion. As in recent works,[20,47] we have implemented a Gaussian-weighted binning procedure for the final assignment of integer ν' and j' values, which was shown to give a better agreement with full quantum mechanical methods than the previously used histogrammatic binning.[47]

IV. RESULTS

A. Doppler-free HD($\nu'=2,j'=1$) E, $F-X$ REMPI measurements

To resolve the ambiguity of the unexpectedly high population in the HD($\nu'=2,j'=1$) state at high collision energies,[12] it was decided to investigate this REMPI transition more closely. Figure 3 presents the collision energy dependence of the population corresponding to this transition over the energy range 1.54–1.89 eV. The relative populations are normalized to the sum of the relative populations in the $j'=0$ and $j'=2$ states. As can be clearly seen, the relative population for the $j'=1$ state essentially lies on a straight line with respect to the populations of the two adjacent states for the lower collision energies of 1.54 and 1.64 eV. This situation is not present, however, for the higher energies of 1.80 and 1.89 eV.

A closer look at the Doppler profiles of the transitions probing the various states illuminates the problem further. The power and baseline corrected signals at $E_{\mathrm{col}}=1.80$ eV are shown in Fig. 4; for HD($\nu'=2,j'=0$) in Fig. 4(a), HD($\nu'=2,j'=1$) in Fig. 4(b), and for HD($\nu'=2,j'=2$) in Fig. 4(c). It is obvious that the HD($\nu'=2,j'=1$) transition line shape is much broader and also slightly asymmetric compared to the line shapes of the neighboring transitions.

The bandwidth of the probe laser is narrower than the Doppler width of the transitions, but not narrow enough to reveal more subtle contributions to the Doppler profiles. Therefore, the next step is to investigate the dependence of the HD($\nu'=2,j'=1$) transition at the higher collision energies as a function of the probe laser bandwidth. Figure 5(a) shows the HD($\nu'=2,j'=1$) transition at $E_{\mathrm{coll}}=1.80$ eV under normal conditions with the probe laser beam having a bandwidth of about 1.0 cm^{-1}. Figure 5(b) shows the same transition using the probe laser in the seeded mode with an estimated bandwidth of 0.3 cm^{-1}.

The observed slight asymmetry is apparent and seems to be caused by the blending of two lines. Changing to a Doppler-free setup (as described in Sec. II) leads to the emergence of a narrow peak at the center wavelength which corresponds to the ionization of the molecules in a specific rovibrational state irrespective of their velocity projection in the direction of the laser beams.[48] It should be noted though, that the narrowing only affects the line broadening caused by the Doppler effect. Other broadening mechanisms, like predissociation or collision broadening, may still contribute to the line shape. The result for one transition will be the sum of the conventional, Doppler-broadend line shape and an additional Doppler-free peak. The effect is more pronounced the more the transition in question is affected by Doppler-broadening. Therefore, it would be expected that in the case of two blended lines two additional lines should emerge in a Doppler-free arrangement with one additional line in the center of each original transition. This behavior is indeed the case [see Figs. 5(c) and 5(d)], but the Doppler-free contribution on the left-hand side of the original peak in Fig. 5(c) is barely visible.

Further verification is obtained by examining a Doppler-

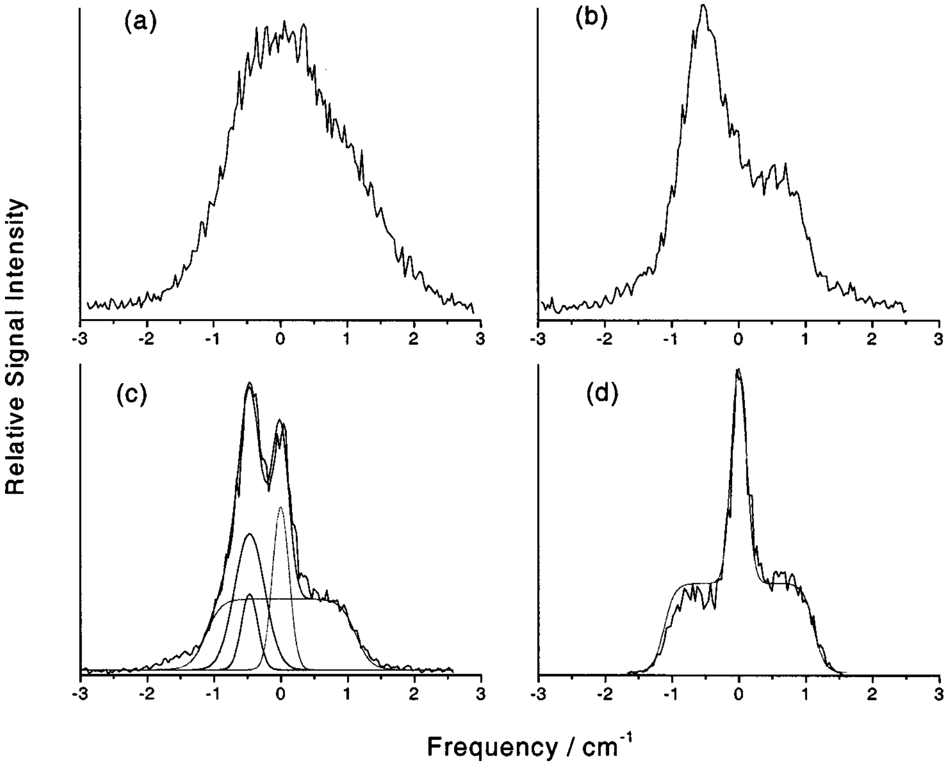

FIG. 5. Effect of the UV probe laser beam bandwidth on the observed transitions: (a) HD($\nu'=2,j'=1$) no seeder (estimated laser bandwidth 1.0 cm^{-1}); (b) HD($\nu'=2,j'=1$) seeded (estimated bandwidth 0.3 cm^{-1}), (c) HD($\nu'=2,j'=1$) Doppler-free scan; and (d) HD($\nu'=1,j'=13$) Doppler-free scan. The latter two are fitted to an expression of Brownswood *et al.* (Ref. 48) for the Doppler-broadened contribution and a Gaussian for the Doppler-free one.

free scan of the HD($\nu'=1,j'=13$) transition. The result is depicted in Fig. 5(d) and the distinct Doppler-free shape on top of the "normal" transition can clearly be seen. The transition was fitted by the sum of an expression for Doppler-broadened lines proposed by Brownswood and co-workers,[49] and a Gaussian to approximate the Doppler-free component. The same functions were also used to fit the HD($\nu'=2,j'=1$) transition depicted in Fig. 5(c). Based on these results and the approximate knowledge of the position of the HD($\nu'=1,j'=14$) transition, it can be concluded that the presence of the REMPI transition involving HD($\nu'=1,j'=14$) confuses the measurement of the HD($\nu'=2,j'=1$) transition at collision energies where a substantial population of the HD($\nu'=1,j'=14$) state is produced. The energetic threshold for the production of this state is at $E_{\mathrm{coll}}=1.54$ eV. Below that collision energy, no disturbance of this state on the observed signal should be present. In principle, the relative population of the HD($\nu'=2,j'=1$) state could be determined by deconvoluting the blended transition into its components. This approach, however, is highly unpractical and difficult using the present laser bandwidth. Instead, a linear interpolation of the population of the HD($\nu'=2,j'=1$) state by using the populations of the HD($\nu'=2,j'=0$) and HD($\nu'=2,j'=2$) states produces a very good approximation within the errors of this experiment. This result can also be used to interpret previous rotational distributions measured outside of the collision energy range of this study.

B. Experimental rotational distributions

Figure 6 displays the observed experimental distributions together with the time-dependent and time-independent quantum mechanical calculations in the collision energy range of 1.30–1.89 eV.

For a collision energy of 1.64 eV or higher a significant interference from the HD ($\nu'=1,j'=14$) product was detected (see above). Therefore, the data for HD($\nu'=2,j'=1$) for collision energies $E_{\mathrm{coll}}\geqslant 1.64$ eV is presented by a linear fit between the HD($\nu'=2,j'=0$) and the HD($\nu'=2,j'=2$) populations, whose REMPI transitions are well behaved. In the case of 1.45 eV, the measurement of the HD($\nu'=2,j'=8$) was not measured reproducibly and is also approximated by a linear fit. These data are denoted in the figures by open squares without error bars. As can be seen in Fig. 6 by the size of the error bars, which represent 1σ, the measurements at low collision energies tend to be less reliable because of the poor signal-to-noise levels. At some low collision energies no reproducible detection of the HD($\nu'=2,j'=0$) product was possible. The population was then set to zero and this is denoted in the figure with an open square but with the respective error bar.

The sum of the population in the rotational levels was normalized to unity in each case and this normalization accounts for some of the discrepancies between the theoretical predictions and the measurements; if one measured point is unusually high or low, it affects the whole distribution through the normalization procedure. In any case, the agreement found between experiment and theory is rather good, especially at the higher collision energies studied in this work.

In addition to the presentation as rotational distributions, the results may also be displayed as surprisal plots[20] as shown in Fig. 7. A summary of the parameters and quantities of these rotational distributions is presented in Table I.

As in our previous work,[20] both the experimental and theoretical results can be presented as $E-j'$ plots (cross section as function of the rotational state and the collision energy in a three-dimensional representation) as shown in Fig.

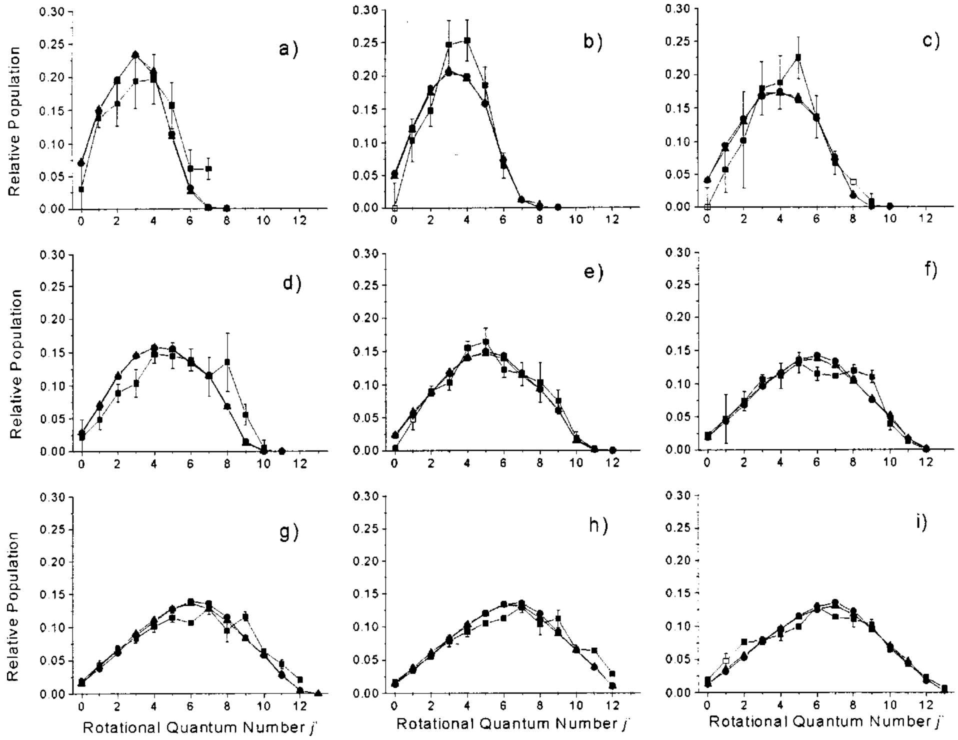

FIG. 6. Rotational distributions at different collision energies: (a) 1.30 eV; (b) 1.35 eV; (c) 1.45 eV; (d) 1.54 eV; (e) 1.64 eV; (f) 1.75 eV; (g) 1.80 eV; (h) 1.85 eV; and (i) 1.89 eV. Squares with error bars denote experimental data, open squares refer to data adjustment as described in the main text. Circles represent the results of the time-dependent quantum mechanical calculations and the triangles the time-independent calculations. All populations normalized to sum to unity.

8. Because no experimental data for the variation of the cross section as function of the collision energy exist for the HD($\nu'=2,j'$) product states, the experimental data were multiplied by the average of the calculated values of the time-independent and time-dependent quantum mechanical results.

One question that arose in our previous work[20] is the effect of the internal state distribution of the D_2 reagents in

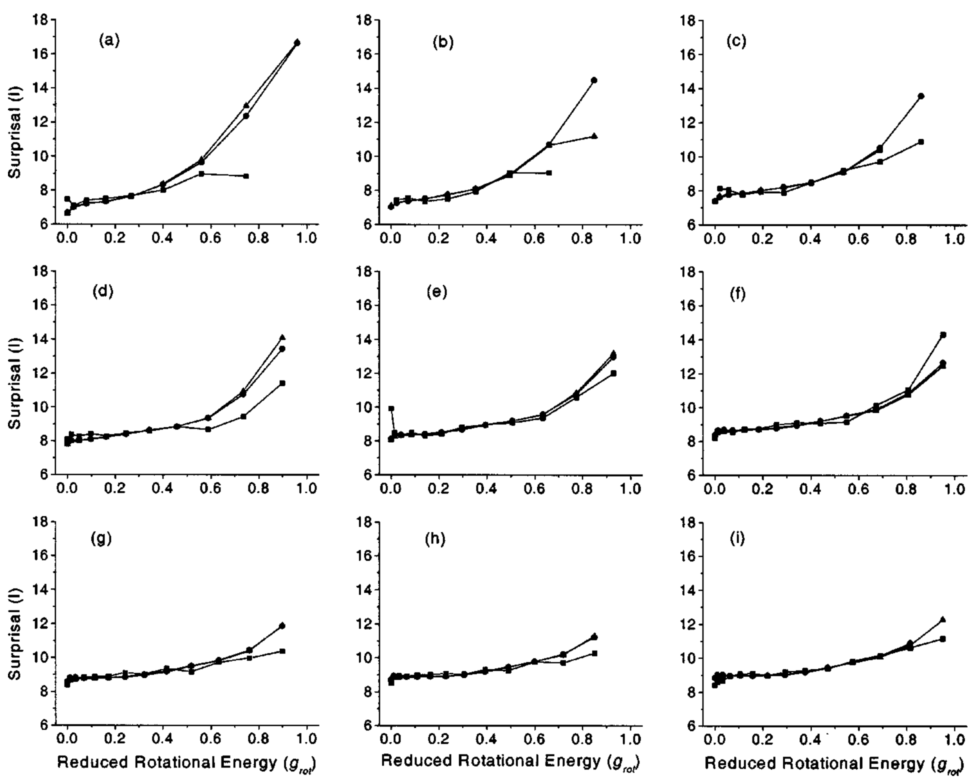

FIG. 7. Surprisal plots for the collision energy range of 1.30–1.89 eV. Symbols and panels as in Fig. 6. g_{rot} denotes the reduced rotational energy.

TABLE I. Summary of rotational parameters for the HD($\nu'=2,j'$) rotational product state distribution as a function of collision energy. "Expt." denotes experimental data, while "Theory" denoted the average of the time-dependent and time-independent calculations. $\langle E_{avail}\rangle$ is the average energy available to be channeled into rotation for this specific vibrational state. Surprisal denotes the slope of the surprisal parameter I against g_{rot}. T_{rot} is derived by equating the sum of rotational energy for a given collision energy to $k_B T$.

E_{coll}/eV	$\langle E_{avail}\rangle$/cm^{-1}	Surprisal		$\langle E_{rot}\rangle$/cm^{-1}		T_{rot}/K		$\langle E_{rot}\rangle/\langle E_{avail}\rangle$	
		Expt.	Theory	Expt.	Theory	Expt.	Theory	Expt.	Theory
1.30	3060	2.4	9.4	744	535	1070	769	0.07	0.05
1.35	3463	3.0	6.2	849	672	1222	968	0.08	0.06
1.45	4269	3.3	4.7	1076	924	1548	1329	0.09	0.08
1.54	4995	2.6	5.2	1493	1161	2148	1677	0.12	0.09
1.64	5802	2.7	4.1	1559	1457	2243	2095	0.12	0.11
1.75	6689	4.4	3.2	1780	1721	2561	2563	0.13	0.13
1.80	7092	1.8	2.8	2119	1924	3049	2768	0.15	0.13
1.85	7496	1.5	2.4	2283	2064	3285	2970	0.15	0.14
1.89	7818	2.4	2.4	2162	2192	3111	3153	0.14	0.14

the molecular beam. The HBr rotational distribution in the molecular beam was measured and a rotational temperature of about 90 K was found to describe it best. This temperature can be taken as being representative for the D_2 rotational distribution as well. A QCT calculation using the Gaussian-weighted binning procedure has been carried out to estimate the effect of the rotational quantum number of the D_2 molecule on the calculated HD($\nu'=2$) product distribution. This effect was found to be negligible. This behavior is clearly demonstrated for two different collision energies in the results shown in Fig. 9, where the HD($\nu'=2,j'$) rotational distributions obtained for the H+D_2($\nu=0,j=0,1,2$) reactions are presented.

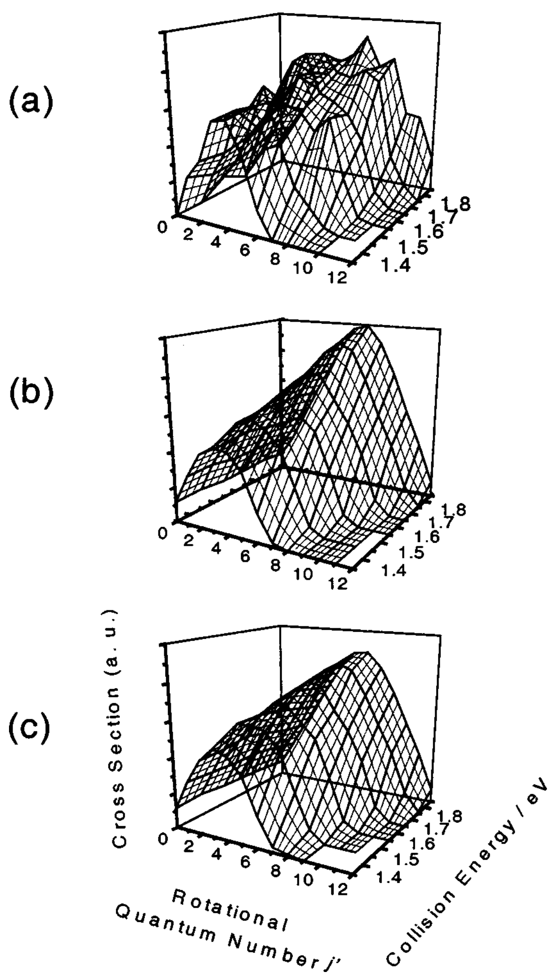

FIG. 8. Relative reactive cross section for HD($\nu'=2,j'$) product as a function of rotational quantum number and collision energy ($E-j'$ plots): (a) the experimental data; (b) time-dependent; and, (c) time-independent quantum calculations. Because no experimental measurement of the integral cross section exists, the experimental data were scaled by the average of the two calculated values.

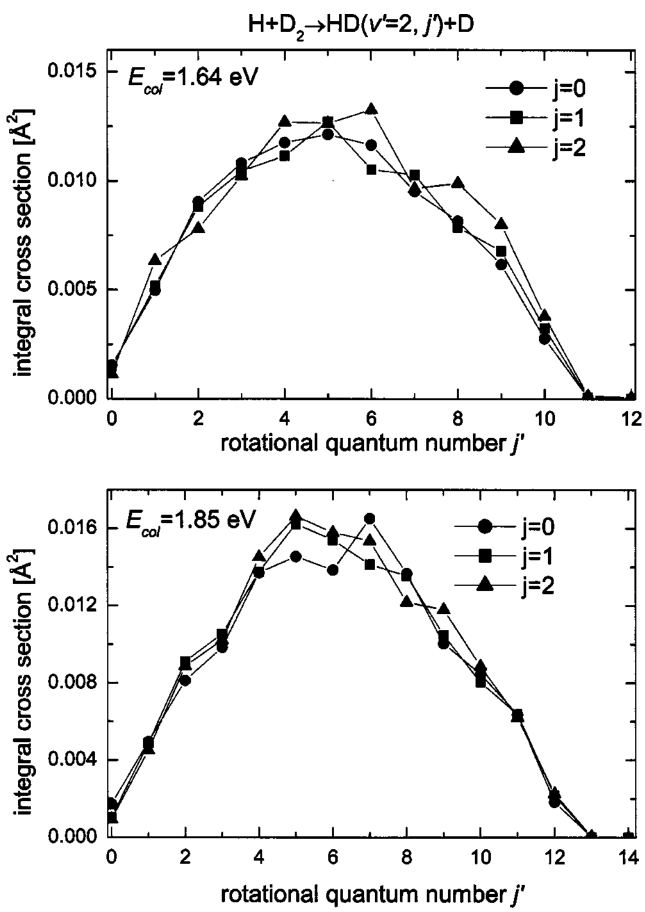

FIG. 9. Quasiclassical trajectory calculations with Gaussian-weighted binning of the HD($\nu'=2,j'$) product state rotational distribution to investigate the effect of the different $D_2(j)$ state populations present in the experimental molecular beam expansion for 1.64 eV (upper panel) and 1.85 eV (lower panel) collision energies.

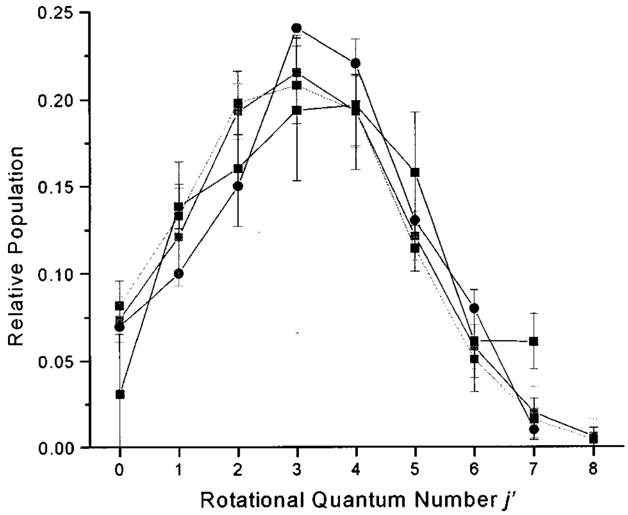

FIG. 10. Comparison with previous experimental observations of the HD($\nu'=2,j'$) product state rotational distribution for $E_{\rm col}=1.30$ eV. The circles denote a measurement using the D-Rydberg-tagging technique (Ref. 24), the squares denote various measurements by REMPI: light gray (Ref. 11) and dark gray (Ref. 13). The closed squares are the data from the present work.

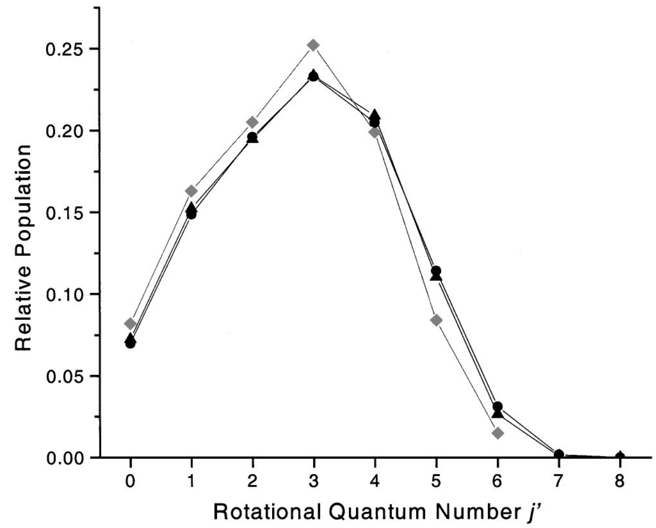

FIG. 11. Comparison with previous theoretical studies of the HD($\nu'=2,j'$) product state rotational distribution for $E_{\rm col}=1.30$ eV. The gray diamonds display an earlier time-independent quantum mechanical study (Ref. 31), while the closed triangles denote the present time-independent and the closed circle denote the present time-dependent study.

V. DISCUSSION

A. General remarks

As can be seen in Fig. 6, the HD($\nu'=2,j'$) distributions calculated by the time-dependent and time-independent quantum methods on the BKMP2 PES are in excellent agreement with each other. Agreement with the experimental data is very good even at low energies, which have the lowest signal levels. The agreement becomes better with increasing collision energy and at the highest collision energies it is nearly quantitative. A similar picture emerges from the suprisal analysis as shown in Fig. 7, where an excellent agreement between the theoretical data and a very good agreement with the experimental values is found. In general, the experiment seems to deviate from the calculations on the high values of the reduced rotational energy ($g_{\rm rot}$) which correspond to the highest j' levels observed in the experiment. These levels have smaller signals and correspondingly higher uncertainties.

At the higher collision energies, both the experimental and theoretical fractions of energy channeled into rotation reach maximum value subject to fluctuations (see Table I). The theoretical values of the slopes of the surprisal, while becoming consistently smaller at the higher collision energies, do not show the preference to approach the statistical limit as that found in our previous study on the HD($\nu'=3,j'$) product rotational distributions.[20] The experimentally derived suprisal parameters do not show any specific trend or preference.

B. Comparison with previous data

Extensive theoretical and experimental work has been carried out for this system. Most of it has focused on the convenient photolysis of HI at 266 nm which produces H atoms corresponding to collision energies of 1.3 and 0.55 eV for the fast and slow channels, respectively. The data beyond 1.3 eV collision energy are too sparse; and therefore, we concentrate our comparison to $E_{\rm coll}=1.3$ eV. Experimentally, data exist from early CARS measurements,[5] several measurements using REMPI,[10,11,13] and data obtained using the D-atom Rydberg-tagging technique.[24] Figure 10 displays data sets for the more recent REMPI, Rydberg-tagging, and present measurements. As can be seen, good general agreement exists among different experimental results available at this collision energy.

On the theoretical side, several QCT studies have been carried out, mainly to test the quality of potential energy surfaces. Two studies are of relevance in this context, both performed on the LSTH surface.[27,32] Additionally, an earlier time-independent quantum-mechanical calculation on the LSTH surface exists.[31] Figure 11 plots this result for comparison with the present theoretical data. The agreement between the previous and current quantum mechanical calculations is striking, especially considering that they were carried out on different surfaces.

C. Comparison with HD($\nu'=3,j'$) rotational distributions

The behavior of the HD($\nu'=2,j'$) rotational distributions as a function of collision energy presented here is in marked contrast with the previous measurements of the HD($\nu'=3,j'$) product rotational distribution as a function of collision energy in essentially the same energy range.[20] The latter showed that experiment and theory deviated, and the deviation became more pronounced with increasing collision energy. The experimental rotational distributions changed qualitatively and became more statistical with increasing collision energy, while the theoretical ones behaved similar to the HD($\nu'=2,j'$) ones presented in this study. This behavior is interesting because for a given collision energy the HD($\nu'=2,j'$) product has more energy available to distribute into rotation than the HD($\nu'=3,j'$) product. In addition, the fraction of rotational energy as a function of collision energy for the HD($\nu'=3,j'$) product showed no propensity to approach a constant value. Instead, it continued to increase over the range of collision energies available. The reason for this different behavior between the two different vibrational states is not yet understood. Because the same experimental technique is used in both studies, it seems unlikely that an experimental error is the source of the disagreement between theory and experiment for the HD($\nu'=3,j'$) product rotational distribution as a function of collision energy. As mentioned previously,[20] the discrepant behavior might be the result of two possibilities. The first is that the formation of HD($\nu'=3,j'$) may occur in a region of the potential energy surface that is more poorly known. The second possibility is that nonadiabatic effects may more strongly influence the production of these higher vibrational levels.

ACKNOWLEDGMENTS

S.C.A. would like to thank the Royal Society for a University Research Fellowship. J.F.C. gratefully acknowledges support by the Spanish Ministry of Science and Technology through a contract within the Ramon y Cajal program. The Spanish group was supported by the Spanish Ministry of Science and Technology (Project No. BQU2002-04627-C02-02) and by the European Commission within the RT Network *Reaction Dynamics* (Contract No. HPRN-CT-1999-00007). The American group gratefully acknowledges funding by the National Science Foundation (NSF CHE 02-42103).

[1] F. Fernández-Alonso and R. N. Zare, Annu. Rev. Phys. Chem. **53**, 67 (2002).
[2] B. K. Kendrick, J. Phys. Chem. **107**, 6739 (2003).
[3] S. C. Althorpe and D. C. Clary, Annu. Rev. Phys. Chem. **54**, 493 (2003).
[4] D. P. Gerrity and J. J. Valentini, J. Chem. Phys. **79**, 5202 (1983).
[5] D. P. Gerrity and J. J. Valentini, J. Chem. Phys. **81**, 1298 (1984).
[6] D. P. Gerrity and J. J. Valentini, J. Chem. Phys. **82**, 1323 (1985).
[7] D. P. Gerrity and J. J. Valentini, J. Chem. Phys. **83**, 2207 (1985).
[8] H. B. Leben, D. L. Phillips, J.-C. Nieh, D. P. Gerrity, and J. J. Valentini, Chem. Phys. Lett. **143**, 317 (1988).
[9] D. V. Lanzisera and J. J. Valentini, J. Chem. Phys. **103**, 607 (1995).
[10] E. E. Marinero, C. T. Rettner, and R. N. Zare, J. Chem. Phys. **80**, 4142 (1984).
[11] R. S. Blake, K.-D. Rinnen, D. A. V. Kliner, and R. N. Zare, Chem. Phys. Lett. **153**, 365 (1988).
[12] K.-D. Rinnen, D. A. V. Kliner, R. S. Blake, and R. N. Zare, Chem. Phys. Lett. **153**, 371 (1988).
[13] K.-D. Rinnen, D. A. V. Kliner, and R. N. Zare, J. Chem. Phys. **91**, 7514 (1989).
[14] D. A. V. Kliner and R. N. Zare, J. Chem. Phys. **92**, 2107 (1990).
[15] D. A. V. Kliner, D. E. Adelman, and R. N. Zare, J. Chem. Phys. **94**, 1069 (1991).
[16] D. A. V. Kliner, D. E. Adelman, and R. N. Zare, J. Chem. Phys. **95**, 1648 (1991).
[17] D. E. Adelman, N. E. Shafer, D. A. V. Kliner, and R. N. Zare, J. Chem. Phys. **97**, 7323 (1992).
[18] D. Neuhauser, R. S. Judson, D. J. Kouri, D. E. Adelman, N. E. Shafer, D. A. V. Kliner, and R. N. Zare, Science **257**, 519 (1992).
[19] J. D. Ayers, A. E. Pomerantz, F. Fernández-Alonso, F. Ausfelder, B. D. Bean, and R. N. Zare, J. Chem. Phys. **119**, 4662 (2003).
[20] A. E. Pomerantz, F. Ausfelder, R. N. Zare, S. C. Althorpe, F. J. Aoiz, L. Bañares, and J. F. Castillo, J. Chem. Phys. **120**, 3244 (2004), preceding paper.
[21] L. Schnieder, K. Seekamp-Rahn, F. Liedeker, H. Sreuwe, and K. H. Welge, Faraday Discuss. **91**, 265 (1991).
[22] E. Wrede, L. Schnieder, K. H. Welge, F. J. Aoiz, L. Bañares, and V. J. Herrero, Chem. Phys. Lett. **265**, 129 (1997).
[23] E. Wrede and L. Schnieder, J. Chem. Phys. **107**, 786 (1997).
[24] L. Schnieder, K. Seekamp-Rahn, E. Wrede, and K. H. Welge, J. Chem. Phys. **107**, 6175 (1997).
[25] L. Bañares, F. J. Aoiz, V. J. Herrero, M. J. D'Mello, B. Niederjohann, K. Seekamp-Rahn, E. Wrede, and L. Schnieder, J. Chem. Phys. **108**, 6160 (1998).
[26] E. Wrede, L. Schnieder, K. H. Welge, F. J. Aoiz, L. Bañares, J. F. Castillo, B. Martinez-Haya, and V. J. Herrero, J. Chem. Phys. **110**, 9971 (1999).
[27] N. C. Blais and D. G. Truhlar, Chem. Phys. Lett. **102**, 120 (1983).
[28] N. C. Blais and D. G. Truhlar, J. Chem. Phys. **83**, 2201 (1985).
[29] N. C. Blais, D. G. Truhlar, and B. C. Garret, J. Chem. Phys. **82**, 2300 (1985).
[30] N. C. Blais and D. G. Truhlar, Chem. Phys. Lett. **162**, 503 (1989).
[31] M. D'Mello, D. E. Manolopoulos, and R. E. Wyatt, J. Chem. Phys. **94**, 5985 (1991).
[32] F. J. Aoiz, V. J. Herrero, O. Puentedura, and V. Sáez Rábanos, Chem. Phys. Lett. **198**, 321 (1992).
[33] B. K. Kendrick, J. Chem. Phys. **114**, 8796 (2001).
[34] P. M. Regan, S. R. Langford, A. J. Orr-Ewing, and M. Ashfold, J. Chem. Phys. **110**, 281 (1999).
[35] M. J. J. Vrakking, A. S. Bracker, T. Suzuki, and Y. T. Lee, Rev. Sci. Instrum. **64**, 645 (1993).
[36] K.-D. Rinnen, M. A. Butine, D. A. V. Kliner, R. N. Zare, and W. M. Huo, J. Chem. Phys. **95**, 214 (1991).
[37] A. E. Pomerantz, F. Ausfelder, R. N. Zare, and W. M. Huo (unpublished).
[38] W. M. Huo, K.-D. Rinnen, and R. N. Zare, J. Chem. Phys. **95**, 205 (1991).
[39] A. I. Boothroyd, W. J. Keogh, P. G. Martin, and M. R. Peterson, J. Chem. Phys. **104**, 7139 {1996).
[40] S. C. Althorpe, J. Chem. Phys. **114**, 1601 (2001).
[41] S. C. Althorpe, F. Fernández-Alonso, B. D. Bean, J. D. Ayers, A. E. Pomerantz, R. N. Zare, and E. Wrede, Nature (London) **416**, 67 (2002).
[42] S. C. Althorpe, J. Chem. Phys. **117**, 4623 (2002).
[43] S. C. Althorpe, Chem. Phys. Lett. **370**, 443 (2003).
[44] S. C. Althorpe, J. Phys. Chem. A **107**, 7152 (2003).
[45] D. Skouteris, J. F. Castillo, and D. E. Manolopoulos, Comput. Phys. Commun. **133**, 128 (2000).
[46] F. J. Aoiz, L. Bañares, and V. J. Herrero, J. Chem. Soc., Faraday Trans. **94**, 2483 (1998).
[47] L. Bañares, F. J. Aoiz, P. Honvault, B. Bussery-Honvault, and J.-M. Launey, J. Chem. Phys. **118**, 565 (2003).
[48] A. E. Pomerantz and R. N. Zare, Chem. Phys. Lett. **370**, 515 (2003).
[49] R. A. Brownswood, M. Hillenkamp, T. Laurent, H.-R. Volpp, and J. Wolfrum, J. Phys. Chem. A **101**, 6448 (1997).